Complex Systems **1** (1987) 791–803

A Poiseuille Viscometer for Lattice Gas Automata

Leo P. Kadanoff
Guy R. McNamara
Gianluigi Zanetti
The Enrico Fermi and James Franck Institutes, The University of Chicago, 5640 South Ellis Avenue, Chicago, IL 60637, USA

Abstract. Lattice gas automata have been recently proposed as a new technique for the numerical integration of the two-dimensional Navier-Stokes equation. We have accurately tested a straightforward variant of the original model, due to Frisch, Hasslacher, and Pomeau, in a simple geometry equivalent to two-dimensional Poiseuille (Channel) flow driven by a uniform body force.

The momentum density profile produced by this simulation agrees well with the parabolic profile predicted by the macroscopic description of the gas given by Frisch et al. We have used the simulated flow to compute the shear viscosity of the lattice gas and have found agreement with the results obtained by d'Humiéres et al. [10] using shear wave relaxation measurements, and, in the low density limit, with theoretical predictions obtained from the Boltzmann description of the gas [17].

1. Introduction

In a now classic paper, Frisch, Hasslacher, and Pomeau [1] proposed a new technique for solving the two-dimensional Navier-Stokes equation based on the implementation of a lattice gas automaton. Their original idea has recently been extended to two-dimensional binary fluids, two-dimensional magnetohydrodynamics, three-dimensional Navier-Stokes, and other interesting problems [4].

Two-dimensional lattice gas automata have been described in great detail in reference 3. We will therefore give only a very short description of the model in order to define the nomenclature used.

Lattice gas automata are based on the construction of an idealized microscopic world of particles living on a lattice. The particles can move on the lattice by "hopping" from site to site. In the specific examples considered in this paper, we allow only hops from a site to its nearest neighbors (a particle may also remain stationary at its current site) and we indicate these motions with the vectors $\vec{C}^{\alpha}$. The $\vec{C}^{\alpha}$ are traditionally interpreted

as the momenta of the particles. (We are using the lattice spacing, the "mass" of a particle, and the simulation time step as fundamental units.) To simplify even further, we suppose that there cannot be more than one particle with a given momentum at a given site. The population at each site can then be represented by an $l+1$ element binary vector, $\{f^\alpha(\vec{x})\}$, where l is the number of nearest neighbors and $\vec{x}$ is the label of a lattice site. We can now define the microscopic number density

$$\hat{\rho}(\vec{x}) = \sum_\alpha f^\alpha(\vec{x}) \tag{1.1}$$

and the microscopic momentum density

$$\vec{\hat{g}}(\vec{x}) = \sum_\alpha \vec{C}^\alpha f^\alpha(\vec{x}). \tag{1.2}$$

The time evolution of the gas is produced by the effect of two alternating steps: the "hopping" phase we described above and a collision phase. In the latter, the $\{f^\alpha\}$ of each site are transformed according to a set of collision rules. The rules can change from site to site or from time step to time step, but in any case they will conserve the microscopic densities $\hat{\rho}$ and $\vec{\hat{g}}$ on each site.

It is possible to construct macroscopic densities from $\hat{\rho}$ and $\vec{\hat{g}}$ by averaging in space and time over appropriate regions. The time evolution of the macroscopic number and momentum densities, ρ and $\vec{g}$, can be expressed, in the appropriate limit, in terms of the conservation laws

$$\partial_t \rho + \partial_k g_k = 0, \tag{1.3}$$

$$\partial_t g_i + \partial_j T_{ij} = 0, \tag{1.4}$$

(where Latin indices now denote Cartesian coordinates). It should be noted that we express the above densities in units of mass and momentum per unit area rather than units of mass and momentum per lattice site, as used by other authors (for instance, [9,10]). We completely ignore all the mathematical difficulties implied in the derivation of equations (1.3) and (1.4) [3], but we note that ρ and $\vec{g}$ in equations (1.3) and (1.4) are intended to be small perturbations from the equilibrium state, $\vec{g} = 0$ and $\rho =$ constant.

The structure of the stress tensor T_{ij} reflects the symmetries of the underlying lattice. Frisch et al. have shown that a hexagonal lattice possesses sufficient symmetry to obtain the right structure for T_{ij}. By this we mean that up to higher derivatives and $O(g^4)$, it is possible to write

$$T_{ij} =$$

$$\lambda(n) g_i g_j + p(n, g^2)\delta_{ij} - \nu(n)(\partial_j g_i + \partial_i g_j - \delta_{ij}\partial_k g_k) - \xi(n)\delta_{ij}\partial_k g_k, \tag{1.5}$$

where the quantities ν and ξ can be interpreted as transport coefficients while λ (which equals 1 for standard Navier-Stokes) arises from the absence of Galilean invariance for the lattice gas [3,13]. In the limit of incompressible flow, equations (1.3) and (1.4) together with the constitutive relation

(1.5), can be rescaled to the incompressible Navier-Stokes equation [3]. Thus, we can interpret this lattice gas as an analog computer capable of solving the two-dimensional incompressible Navier-Stokes equation.

Note that nowhere is there an attempt to simulate the microscopic behavior of a real fluid. Lattice gas automata are quite distinct from molecular dynamical simulations [20]. While both kinds of simulations seem to produce the expected macroscopic behavior for the fluid (in the sense of giving the expected constitutive relations for the macroscopic currents), they represent two completely different approaches to the problem. Molecular dynamical simulations attempt to faithfully model the microscopic behavior of a real fluid, while lattice gas automata extract only the minimal microscopic properties required to obtain the desired macroscopic behavior [5–7].

This suggests two interesting paths of research. The first, more technically oriented, concerns how well the results obtained from this new technique agree with real fluids, while the second concerns the more profound question of the connection between the microscopic and macroscopic aspects of many body systems [21]. In this paper, we principally address technical questions: the quantitative accuracy of the constitutive relation, equation (1.5), in a particular simple example, and the comparison of the effective kinematic viscosity measured in our steady non-equilibrium simulation with the values obtained by shear wave relaxation methods.

2. The simulation model

The object of our simulation is a steady forced flow between two walls with no-slip boundary conditions. We are simulating a steady flow because it allows us to obtain good accuracy in the measurements of ρ and $\vec{g}$ by extensive time averaging. We are simulating a channel with null velocity at the walls because for weak forcing (low Reynolds number), the g profile is expected to be a parabola and there is a simple relation between the maximum g, the forcing level, and kinematic viscosity ν. The actual simulation setup described below is conceptually very different from a direct implementation of a no-slip boundary channel flow but, as we will show, gives the same parabolic momentum profile.

The simulation system we have employed is a model of forced two-dimensional Poiseuille flow [13,22–24]. The system is a hexagonal lattice with an equal number of rows and columns (figure 1). Note that the system width, W, is $\sqrt{3}/2$ times the length, L, due to the unequal row and column spacings. The flow is forced by adding momentum in the positive x direction to the system at a constant rate: After each time step, we randomly select a lattice site and, if possible, apply one of the microscopic forcing rules described in figure 2. Each successful application of a forcing rule adds one unit of momentum to the system. The forcing process is repeated until the desired amount of momentum has been transferred to the gas; fractional amounts of momentum to be added to the system are accumulated across

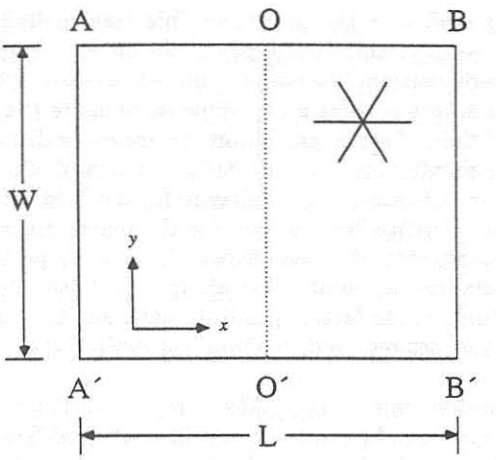

Figure 1: The simulation model. The walls AA′ and BB′ are joined by periodic boundary conditions while "Möbius strip" boundary conditions (see text) are used to connect the AB and A′B′ walls. The representative lattice site shown in the upper right-hand corner illustrates the orientation of the underlying hexagonal lattice.

time steps until they sum to an amount greater than 1, at which time one additional unit of momentum is added to the gas. The result of this process is a constant body force applied to the gas uniformly across the width and length of the channel.[1]

The forcing level employed in the present work varies from 0.3 to 2.8 units of momentum per time step. Within this range, the resulting flow is steady when averaged over a period of the order of a few diffusion times, L^2/ν. For a steady flow, the equations for the forced flow [22,3] become

$$0 = \partial_k g_k \tag{2.1}$$

$$\partial_k(\lambda g_k g_l) = -\partial_l p + \partial_k(\nu \partial_k g_l) + f_l \tag{2.2}$$

where $\vec{f} = (f, 0)$ is the average force per unit area.

The two walls perpendicular to the flow, AA′ and BB′ in figure 1, are mapped onto each other by periodic boundary conditions. The walls parallel to the flow, AB and A′B′, are mapped onto each other by "Möbius strip" boundary conditions. This boundary condition can be described as a two-step process whereby particles crossing the boundary have their position

[1]The actual forcing scheme is slightly more complicated since it must compensate for inhomogeneity in the momentum and number densities due to the macroscopic flow (see [11]). The forcing algorithm randomly selects a lattice row and column and then searches along the row until it finds a site where a forcing rule may be successfully applied. The program terminates if no forcing operation can be performed on a selected row. This guarantees that forcing operations will be uniformly distributed across the width of the channel, despite variations in the mass and momentum densities.

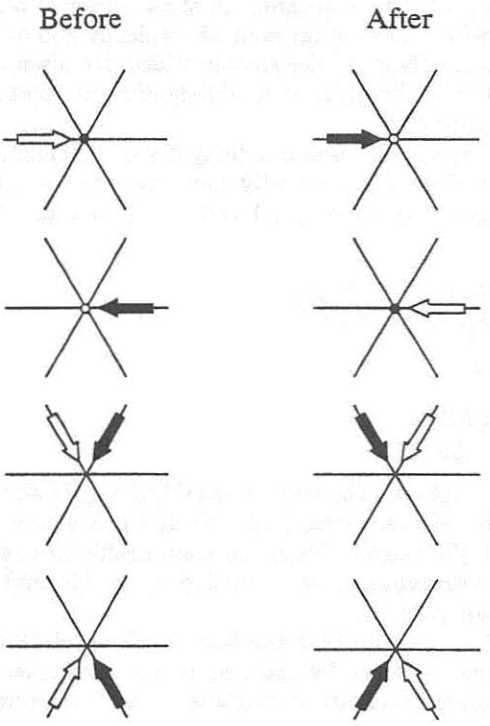

Figure 2: Forcing rules. The four pairs of diagrams represent the microscopic forcing rules used in the simulation. The black symbols indicate occupied states while the outlined symbols indicate vacant states. States not indicated in a diagram may be either filled or vacant. Each forcing operation adds one unit of momentum in the x direction.

and velocity reflected with respect to the line OO′ and then standard periodic boundary conditions are applied. The alternative to the Möbius strip boundary would be the use of no-slip boundary conditions, for instance, random scattering of the particle impinging on the walls. Both boundary conditions dissipate the momentum injected into the gas by the uniform body force, but the no-slip condition creates a layer at the boundary (a Knudsen layer [14]) whose thickness is of the order of a mean-free path.[2] Since the mean-free path for our model is typically about 5 lattice spacings and the system is only 32 lattice rows in width, Knudsen layers along both the upper and lower boundaries would significantly distort the Poiseuille flow momentum profile.

The combination of a uniform body force directed in the positive x direction and vanishing fluid velocity along the upper and lower boundaries gives rise (through equations (2.1) and (2.2)) to a parabolic momentum density profile

$$g_x(y) = \frac{g_{max}}{(\frac{W}{2})^2}(y^2 - (\frac{W}{2})^2), \tag{2.3}$$

with $g_y = 0$ and

$$g_{max} = \frac{1}{8}\frac{FW}{L\nu} \tag{2.4}$$

where we have neglected the corrections $O(g_x(\partial_y g_x)^2)$ due to variation of ρ across the width of the system (see [11]) and y is measured from the axis of the channel. We extract this momentum profile from the simulation by averaging the microscopic momentum density in time and along the lattice rows (lines of constant y).

At this point, we note that the flow which develops in the channel is equivalent to that obtained by applying to a system of length L and width $2W$, with periodic boundary conditions in both directions, the "square wave" force field

$$\vec{f}^*(x,y) = (f,0) \quad \text{for } 0 \le y < W, \tag{2.5}$$

$$\vec{f}^*(x,y) = (-f,0) \quad \text{for } W \le y < 2W. \tag{2.6}$$

We have verified this correspondence by comparing simulation results from runs employing Möbius strip boundary conditions with runs using square wave forcing (see figure 3). Both types of flow exhibit long wavelength instabilities related to the existence of inflection points in the momentum profile at $y = 0$ and $y = W$. The critical Reynolds number given by linear stability analysis for infinitely long channels (Kolmogorov flow [15,16]) is quite small, $Re_{cr} \approx 1.11$, but a finite length-to-width ratio increases Re_{cr}. The particular length-to-width ratio used in our simulation, $1/\sqrt{3}$,

[2] The Knudsen layer is caused by the matching between the artificial particle distribution imposed by this kind of boundary condition and the non-equilibrium particle distributions imposed by the macroscopic flow in the bulk.

appears to be stable even for the largest Reynolds number obtainable in our simulation (≈ 50), as was suggested by the linear stability analysis of the problem.

3. Results

In this section, we will occasionally refer to mass density in number of particles per site $n, n = (\sqrt{3}/2)\rho$, instead of number of particles per unit area, ρ; this is done for notational convenience. Figure 4 shows a typical momentum profile obtained from our simulation. The average number of particles per site in this run is $n = 2.1$, the system dimensions are $W = 16\sqrt{3}$ and $L = 32$ (corresponding to a 32×32 lattice), and we have used the model-II collision rules described in reference 3. The profile was obtained by averaging the microscopic momentum density $\vec{g}$ in the direction parallel to the flow and on one million iterations. The g_y component appears to be due entirely to statistical noise; it is small: $\max |g_y(y)/g_{max}| < 0.01$, where g_{max} is g_x at the center of the channel.

The solid line represent a parabola fitted to the simulation results which are shown as symbols. The fit is very good; if we define

$$e(y) = \frac{|g_x(y) - h(y)|}{g_x(y)}$$

where $h(y)$ is the fitted parabola, then $\max |e(y)| < 0.01$ over the central region of the parabola (roughly the 26 centermost rows).

The result quoted above can be improved by increasing the number of time steps on which the simulation in figure 4 is averaged. However, improvements obtained by averaging are limited by systematic deviations from a parabolic profile which can be reduced only by decreasing the amplitude of $\vec{g}$. These systematic deviations are due to higher-order terms, $O(g^4)$, neglected in equation (1.5), and to the presence of a term proportional to g^2 in the expression, derived in [1,2,3]; for the pressure p, see [11].

We can use equation (2.4) to relate the maximum measured velocity to the applied force. This permits us to define an effective kinematic viscosity

$$\nu = \frac{1}{8}\frac{FW}{Lg_{max}}. \tag{3.1}$$

In figure 5, we plot the measured ν as a function of the reduced density for a set of simulations using the model II collision rules of reference 3. The system used for the measurement was 32×32, and the forcing level was very weak, so that the typical Mach number, defined as the ratio between the speed of sound and the hydrodynamical velocity, $\vec{g}/\rho$, is approximately ≈ 0.1.

In the same figure, we compare our viscosity measurements with data obtained by relaxation measurements [10]. The errors bars for the latter set of data are set at about 3 percent of the actual measured viscosity [12], while the errors on our data set are about 1 percent and are not indicated.

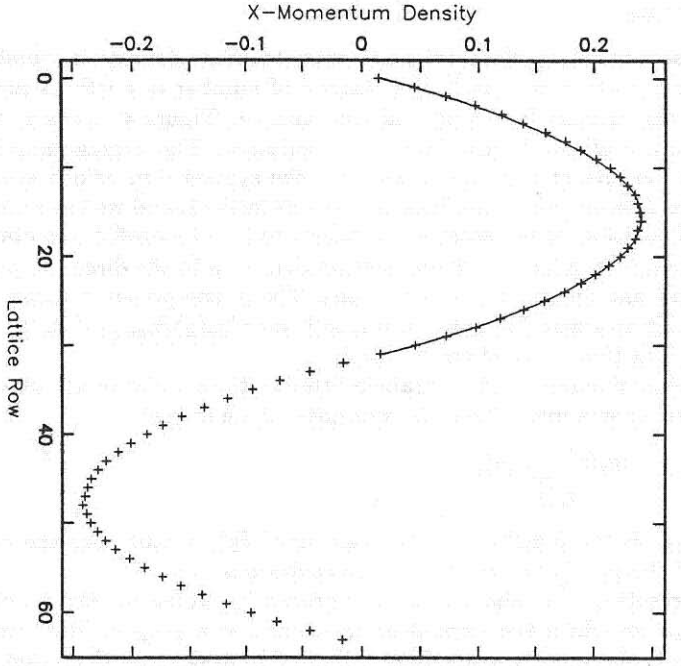

Figure 3: Möbius strip boundary conditions versus square wave forcing. The symbols represent the x momentum density profile for square wave forcing (see text) with periodic boundary conditions in both directions. The solid line is a parabolic fit to the momentum density profile obtained using Möbius strip boundary conditions on a system half as wide. Both simulations were run at a density of 2.1 particles per site and the profiles were averaged over one million time steps.

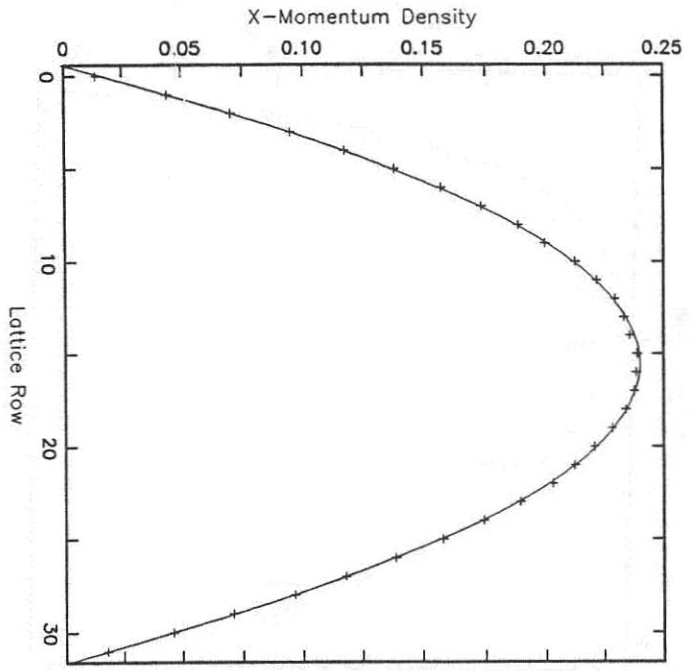

Figure 4: Typical momentum profile. The x momentum density profile for a 32×32 system run at $n = 2.1$ particles per site and a forcing level $F = 0.76$ momentum units per time step. The profile was averaged over one million time steps. The solid line is a parabolic fit to the simulation data points (symbols).

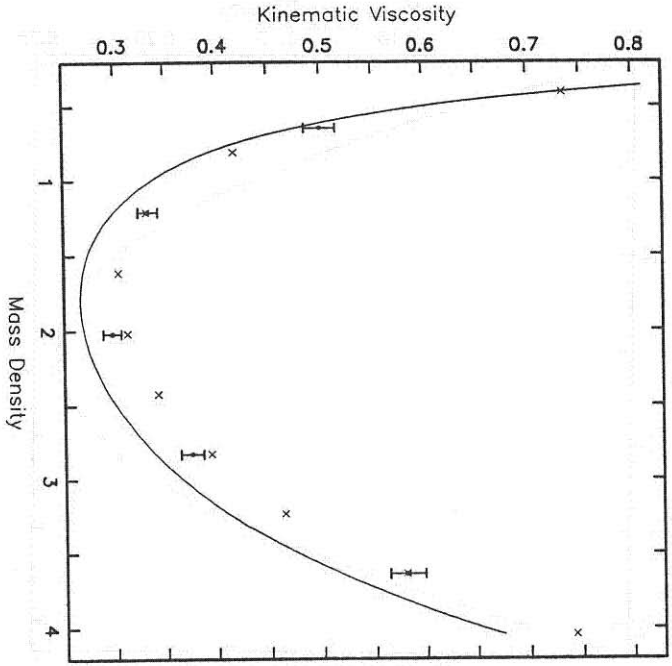

Figure 5: Kinematic viscosity versus mass density. Viscosity values derived from the present work are shown as crosses. Symbols with error bars are the results obtained by d'Humières et al. The solid line is the theoretical value obtained using Chapman-Enskog techniques.

In both cases, the errors are only rough estimates since they were not computed from first principles but were estimated by comparing similar runs with different initial conditions.

The two sets of viscosity data appear to be consistent, except in the range $2 < \rho < 3$, where our data are consistently greater than the results of reference 10. It would be tempting to relate the discrepancy between the two viscosities to viscosity renormalization effects [18], but we presently do not have any conclusive evidence.

The solid line is the shear viscosity as calculated by the technique of Michel Hénon [25] and by other authors using Chapman-Enskog techniques [17]. Both methods are based on an approximate theoretical description of the gas in which the correlations between particles are completely neglected.

In the low density limit, there is a very good agreement with the theory, as is expected since the relative importance of particle correlation becomes negligible in that limit. Note that we do not quote results for $\rho < 0.4$ because for these densities the mean-free path (see [22]) of the particles becames comparable to the width of the channel.

4. Conclusion

We have given some precise simulation evidence that LGAs are correctly represented by the constitutive relation, equation (1.5). We have also shown that the simulation of channel flow gives the expected parabolic profile to a good degree of accuracy and that the effective kinematic viscosity obtained by these steady non-equilibrium flows is in reasonable agreement with that obtained by d'Humières et al. using shear waves relaxation measurements.

The technique used for these simulations is capable of providing reasonably accurate measurement of viscosity; the particular kind of boundary conditions used allow a wide range of lattice size width and makes feasible the study of the dependence of the kinematic viscosity on the width of the simulation channel. For two-dimensional fluids, there are rather precise predictions, based on renormalization group arguments and other techniques, for this dependence [18]. In first-order perturbation theory, the kinematic viscosity diverges as the logarithm of the box size. We have some preliminary results, to be published elsewhere, which indicate the presence of this effect even within the range of channel widths accessible by our method of simulation.

Acknowledgments

We would like to thank B. Hasslacher and U. Frisch for interesting and helpful discussions, and G. Doolen and T. Shimomura for the original version of the FORTRAN program we have used. This work was supported by ONR and NSF-MRL, and we gratefully acknowledge the hospitality of the Los Alamos National Laboratory, where a portion of this work was done.

References

[1] U. Frisch, B. Hasslacher, and Y. Pomeau, *Phys. Rev. Lett.*, **56** (1986) 1505.

[2] S. Wolfram, *J. Stat. Phys.*, **45** (1986) 471.

[3] U. Frisch, D. d'Humières, B. Hasslacher, P. Lallemand, Y. Pomeau, and J. Rivet, "Lattice Gas Hydrodynamics in Two and Three Dimensions", *Complex Systems*, **1** (1987) 648.

[4] See the bibliography of [3].

[5] L. P. Kadanoff and J. Swift, *Phys. Rev.*, **165** (1968) 310.

[6] J. Hardy and Y. Pomeau, *J. of Math. Phys.*, **13** (1972) 1042.

[7] J. Hardy, O. de Pazzis, and Y. Pomeau, *J. of Math. Phys.*, **14** (1973) 1746; *Phys. Rev.*, **A13** (1976) 1949.

[8] D. d'Humières, P. Lallemand, and U. Frisch, *Europhys. Lett.*, **2** (1986) 297.

[9] D. d'Humières, Y. Pomeau, and P. Lallemand, *C. R. Acad. Sci. Paris II*, **301** (1985) 1391.

[10] D. d'Humières, P. Lallemand, and T. Shimomura, "Computer simulations of lattice gas hydrodynamics", LANL preprint.

[11] J. Dahlburg, D. Montgomery, and G. Doolen, "Noise and Compressibility in Lattice-Gas Fluids", *Physical Review*, in press.

[12] D. d'Humières, personal communication.

[13] D. d'Humières and P. Lallemand, *C. R. Acad. Sci. Paris II*, **302** (1985) 983.

[14] C. Cercignani, *Theory and Application of the Boltzmann Equation*, (New York, Elsevier, 1975).

[15] L. D. Meshalkin and Ya. G. Sinai, *J. Appl. Math. (PMM)*, **25** (1979) 1700.

[16] Z. S. She, "Large scale Dynamics and Transition to Turbulence in the Two-dimensional Kolmogorov Flow", *Proceed. Fifth Intern*, Beer-Sheva Seminar on MHD Flows and Turbulence, Israel, March 2–6, 1987.

[17] J. P. Rivet and U. Frisch, *C. R. Acad. Sci. Paris II*, **302** (1986) 267.

[18] Y. Pomeau and P. Résibois, *Phys. Rep.*, **19** (1975) 63.
K. Kawasaki and J. D. Gunton, *Phys. Rev.*, **A 8** (1973) 2048;
D. Forster, D. Nelson, and M. Stephen, *Phys. Rev.*, **A 16** (1977) 732;
T. Yamada and K. Kawasaki, *Prog. of Theor. Phys.*, **53** (1975) 111; Y. Pomeau and P. Résibois, *Phys. Rep.*, **19** (1975) 63.

[19] B. Alder and T. Wainwright, *Phys. Rev. Lett.*, **18** (1970) 968.

[20] D. J. Evans and G. P. Morriss, *Phys. Rev. Lett*, **51** (1983) 1776; D. H. Heyes, G. P. Morriss, and D. J. Evans, *J. of Chem. Phys.*, **83** (1985) 4760.

[21] L. P. Kadanoff, *Physics Today*, **39** (1986) 7.

[22] C. Burges and S. Zaleski, "Buoyant Mixtures of cellular Automaton Gases", *Complex Systems*, **1** (1987) 31.

[23] K. Balasubramanian, F. Hayot, and W. F. Saam, "Darcy's law for lattice gas hydrodynamics", Ohio State University preprint (1987).

[24] D. H. Rothman, MIT preprint (1987), submitted to *Geophysics*.

[25] M. Hénon, *Complex Systems*, **1** (1987) 762.